J Nanostruct 10(2): 198-205, Spring 2020

RESEARCH PAPER

Size-Controlled Synthesis of Gold Nanostars and Their Characterizations and Plasmon Resonances

Mehrdad Monsefi [1], *Tahoora Tajerian* [1*], *and Alan Rowan* [2]

[1] *Department of physics, Karaj branch, Islamic Azad University, Karaj, Iran*

[2] *Australian Institute for Bioengineering and Nanotechnology, The University of Queensland, Brisbane QLD 4072 Australia*

ARTICLE INFO

Article History:
Received: 29 October 2019
Accepted: 24 February 2020
Published: 01 April 2020

Keywords:
Au seed
Capping agent
Gold nanostar
Plasmonic peak
Reduction

ABSTRACT

Gold nanostar particles were synthesized using seed-mediated method. Au-seed was synthesized with the diameter of approximately 3 nm and a considerably low STDEV of less than 1 nm. Then, different amount of Au seed was introduced into the growth solution of nanostars and the influence of the changes in concentration of Au seed on the growth process was investigated. The size of gold nanostars increased with decreasing the concentration of Au seeds. We further extended this method to enable size-control of gold nanostars from approximately 70 nm to 140 nm in size. Also the longer branch length caused red shifting of resonant plasmonic peaks in the absorption spectra of the sample with the lower amount of Au seed. Thanks to this method, we could control size, and spikes of gold nanostars and the obtained results broaden the concept of the formation and morphology of gold nanostars. The plasmon band shift was attributed to variations in branch numbers, and overall star size.

How to cite this article
Monsefi M, Tajerian T and Rowan A. Size-Controlled Synthesis of Gold Nanostars and Their Characterizations and Plasmon Resonances. J Nanostruct, 2020; 10(2):198-205. DOI: 10.22052/JNS.2020.02.001

INTRODUCTION

Star-shaped nanoparticles as plasmonic materials have achieved a huge interest among many existing anisotropic gold nanostructures due to their applications in light based technologies [1]. Gold nanostar (GNS) particles can have special shapes, such as sharp tips and edges which can highly concentrate light [2-4]. The ability of confining light at nanoscale dimensions provides gold nanostructures with numerous unique properties, including large electromagnetic field enhancements, high photothermal conversion efficiencies and rich spectral responses [5-6]. As a result, they are one of the most promising candidates for tuning the plasmonic peak and for use in many applications such as: surface enhanced Raman spectroscopy (SERS), chemical sensors, second harmonic generation (SHG) [7-8], photonics [9-10], biological sensing [11-13], and in vivo biomedical optical imaging [9,14].

The Vis-NIR spectra of GNSs show a peak that gives rise to a main localized surface plasmon resonance (LSPR) band [15]. Many parameters in the seed-mediated synthesis of GNSs such as pH, seed concentration and size, ascorbic acid concentration, temperature, and the surfactant's concentration influences the shape, number of branches, and the plasmonic peak of GNSs. The possibility of tuning the plasmon band of anisotropic nanoparticles to be in resonance with near-infrared light source is an essential feature, affording excellent opportunities toward biological applications [16-17]. Numerous reports have described the growth kinetics of GNS's however the size issue and its corresponding plasmonic peak intensity have still potential to be proposed.

* *Corresponding Author Email: tahoorataj@gmail.com*

In this research, a seed meditated technique that was pioneered by Jana and Murphy et al. [18-19], has been used to fabricate four different types of nanostar particles and the possibility of tuning the morphology of GNSs has been presented. The advantage of our method was the ability to vary size and morphology resulting in variation in LSPR spectrum of the GNS particles.

MATERIALS AND METHODS

Materials and instrumentation

In order to fabricate gold nanostar (GNS), the following reagents were used in both seed and growth section of experiments: chloroauric acid ($HAuCl_4$, Mw = 393.83 gr/mol, Acros-Organics), trisodium citrate ($Na_3C_6H_5O_7$, Mw = 294.10 gr/mol, Merck), sodium borohydride ($NaBH_4$, Mw = 37.83 gr/mol, Fluka), silver nitrate ($AgNO_3$> = 99.0%, Mw= 169.87 gr/mol, SIGMA-ALDRICH), ascorbic acid (or AA, $C_6H_8O_6$, 99% A.C.S, Mw= 176.12 gr/ml, SIGMA-ALDRICH) and cetyltrimethylammonium bromide (or CTAB, $C_{19}H_{42}BrN$, Mw = 364.45 gr/mol, TIC Europe nu). For the preparation of all solvents, pure water (Milli-Q water, MQ 18.1 MΩ) was used. All the reagents were used without any additional purification, and all the reused glassware was cleaned with hydrochloric acid (HCl) and nitric acid (HNO_3) with 3:1 ratio. Sonication was carried out with an ultrasonic bath (Branson Ultrasonic Cleaner 2520E-DTH) and centrifugation was performed with a Scan Speed (1730R) centrifuge. A UV-vis-NIR spectrophotometer (Varian-Cary-50 Conc.) has been used as well for measuring the nanoparticles absorption spectra. In order to investigate the morphology and size of the particles, a transmission electron microscopy (TEM-JEOL1010) was used. A nanoparticle size and concentration analyzer (NANO sight-NS500) was used to analyze the size distribution of nanoparticles in liquid.

Citrate-capped seed synthesis

Citrate-capped seed was synthesized in presence of $NaBH_4$, a strong reducing agent, to reduce Au^{+3} to Au^o. The synthesis was carried out based on the reaction (1) and the methodology described in [18-20].

$$6H_2O + 8AuCl_4^- + 3NaBH_4 \rightarrow 8\,Au^o + 3\,HBO_2 + 3\,NaCl + 29\,HCl \quad (1)$$

Citrate was present as a capping agent and stabilizer to prevent the final Au seed from aggregation. The process started via preparation of 20 ml aqueous solution containing 10 ml of $HAuCl_4$ (250 µM) and 10 ml of $Na_3C_6H_5O_7$ solution (250 µM). Pouring it into an Erlenmeyer flask that was cleaned and equipped with a proper magnetic stirrer (6×20 mm) inside and then stirring for 10 min were the next stage. Then 600 µl of ice cold $NaBH_4$ solution (0.1 M) was added (chilled 30 min in the ice bath). The solution immediately turned orange-red, indicating the formation of gold nanoparticles. Au seeds are ready to use after approximately 2 hours for preparation of gold nanostars in the next stage.

Growth solution syntheses

Fabrication of gold nanostars was carried out with variations in the amount of Au seeds with a sequenced mentioned in the following. The inside reaction in terms of electron donation can be interpreted as the formulas (2) to (4) [21-22].

$$AuCl_4^- + 4CTAB \leftrightarrow CTA - AuBr_4 + 4Cl^- + 3CTA^+ \quad (2)$$

$$CTA - AuBr_4 + C_6H_8O_6 \rightarrow AuBr_2 + C_6H_6O_6 + 2H^+ + 2Br^- \quad (3)$$

$$2CTA - AuBr_2 + C_6H_8O_6 \rightarrow 2Au + C_6H_6O_6 + 2CTA^+ + 2H^+ + 4Br^- \quad (4)$$

CTAB is an ionic long-chained molecular solvent used as growth solution and which also acts a shape directing agent. The only reagent missing in the solution is CTAB, since its volume in the growth solution is incomparable to the rest ($V_{CTAB} \gg V_{other\ reagents}$). In the presence of the Au seed, it would lead to the growth of particles with the desired star-shaped or hyper-branched morphology.

Table 1 shows the concentration of each

Table 1. Represented percentage of the reagents in the synthesis.

Chemicals	Sample 1	Sample 2	Sample 3	Sample 4
Au (10 mM)	59.3%	59.3%	59.3%	59.3%
Ag (10 mM)	14.8%	14.8%	14.8%	14.8%
Au seed	3.7%	2.4%	1.9%	1.2%
AA (100 mM)	22.2%	23.5%	24.0%	24.7%

reagent used in the growth solution of gold nanostars. Four amounts of Au seed concentration in percentage units were carried out in order to obtain the influence of Au seed's ratio on the size, number of branches and the plasmonic wavelength of the respective samples. A mixture of CTAB solution (0.1 M) with $AgNO_3$ (10 mM) and $HAuCl_4$ (10 mM) was prepared at first and stirred mildly for 1 minute. Wrapping the silver solution with aluminum foil was necessary to avoid any oxidation by light. Then a sonication for 45 minutes in 45 °C degree was done. The solution should be kept under the same condition during the experiment. Ag attached to the bromide (Br) on the CTAB to form AgBr. AgBr changed the Au seed particles into asymmetrical forms and the growth of GNS's continued in the presence of the long-chained CTAB molecules [23-24]. Introducing 100 mM of AA to the growth solution in the final step caused transferring electrons to the Au seed and reduction of the Au ions and formation of a gold shell around the asymmetrical seed. Because of the presence of CTAB, a careful centrifuging was needed. It was done with 3500 rpm for 5 minutes followed by 1300 rpm for 15 minutes. Subsequently, washing the samples with a MQ was required. The final solutions were transferred into the Cubi-fridge for an incubation period of 3 hours and four different dark blue solutions resulted after the complete formation of GNS particles. Four types of GNS particles formed called as GNS1 to GNS4; however there were some differences in the final solutions i.e. color of them due to their size, length/width of spikes (branches) and additionally their plasmonic spectra. This uniformity would facilitate further research or even functionalization on the final products.

RESULTS AND DISCUSSION

Fig. 1a shows the formation of Au seed in the presence of capping agent and subsequently Fig. 1b schematically demonstrates the growth of star-shape nanoparticles in the presence of CTAB and breaking role of silver in GNS formation. AgBr leads to asymmetrical seed particles and growth of the GNS continues in the presence of the long-chained CTAB molecule. The Au seed particles have been shown in Fig. 2a. The orange-red color of the solution indicates the formation of gold nanoparticles. The solution scattered light highly due to their particles small size, so they looked very bright. The blue color of the Figs. 2b to 2e is an indication for the formation of gold nanostars. The dark blue spectrum of the final solutions is due to similarities in their shape and spikes numbers. It is also good to be noted that there is

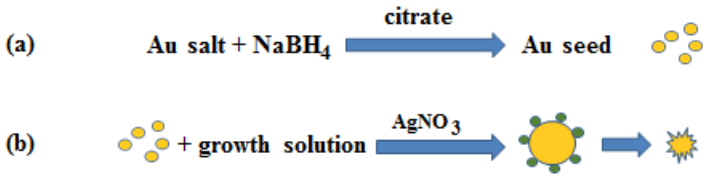

Fig. 1. (a) Schematic formation of Au-seed in the presence of capping agent, and (b) role of silver in the formation of GNS.

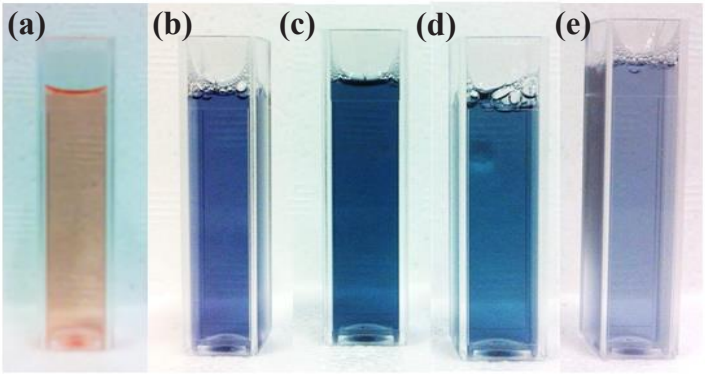

Fig. 2. Final colors of (a) Au-seed solution, (b) GNS1, (c) GNS2, (d) GNS3, and (e) GNS4.

a slight difference in the blue spectrum color of the final solutions; these changes would shift the plasmonic peak as well. The color dissimilarities are arising from deviations in the size, shape and, compositions of nanoparticles. Additionally, the average distance between neighboring gold nanoparticles (yield) plays role in the variety of colors and optical properties of particles. The deviations in the aspect ratio of the nanoparticles in terms of their longitudinal oscillation, even minor changed from spherical geometry would lead to impressive color changes.

Fig. 3a shows a TEM image of Au seed that confirms the formation of gold nanoparticles. Over 100 particles were counted to obtain a statistically accurate representation of the average diameter of the seed. The histogram of the seed particle diameter is presented in Fig. 3b. The average diameter of the particles was found to be 6 nm with a mean value of 7.88 nm and standard deviation (STDV) of 2.53 nm. The inconsistency and the broadness in size distribution may explain the broadness of the plasmonic peak for Au seed spectra. Figs. 4a to 4d show the TEM images of

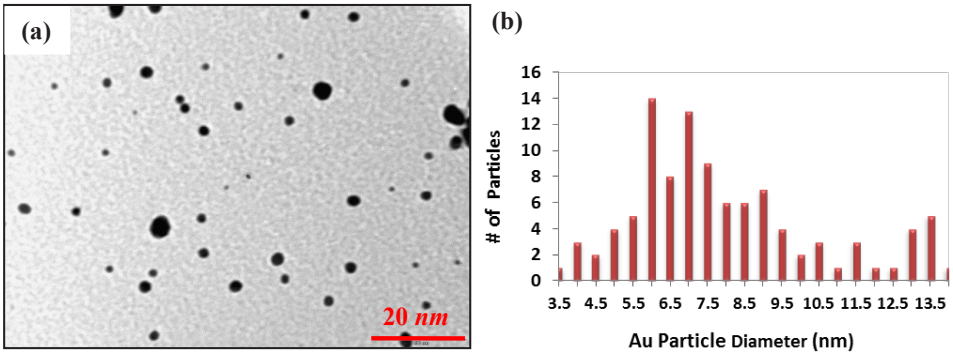

Fig. 3. (a) TEM image of the Au-seed particles, and (b) size distribution histogram of Au-seed particles.

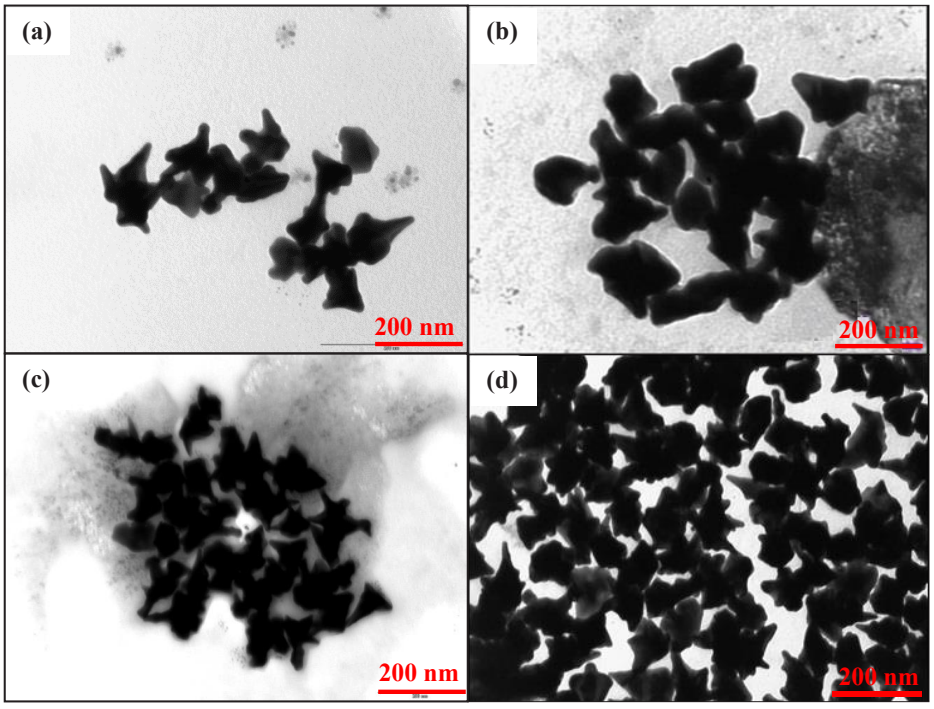

Fig. 4. TEM images of (a) GNS1 (b) GNS2, (c) GNS3, and (d) GNS4.

Table 2. Detailed features of the GNSs.

	GNS1	GNS2	GNS3	GNS4
Wavelength (nm)	593	634	667	672
Number of branches	3	4	4	5
Aspect ratio (AR)	1.4	1.4	1.3	1.4
Dispersion in size (nm)	50	40	60	70
Maximum size (nm)	70-80	110	120	140

gold nanostar sample GNS1 to GNS4. Because of the asymmetry of the particles shape, they were counted manually. The differences in GNS's TEM images presented in order to exhibit particles yield (from low to high), maximum size (from 70 to 140 nm), and the number of branches shape (3 branches to 5).

The detailed differences between particles have been described in table 2. Absorption spectra of the seed and GNS samples were measured as they have been shown in Fig. 5. As the aspect ratios of the samples are similar, so drawing any conclusion about them is difficult. Additionally, increases in size and the maximum length and width of the particles leads to the wavelength red shifting as it was expected in LSPR. However, main deviations in the particle spectrum were in their size and number of the branches, i.e., GNS1 maximum size was 70 nm and it had 3 branches with the LSPR wavelength of 593 nm. The GNS2 maximum size was 110 nm with 4 branches and 634 nm in its LSPR wavelength. The GNS3 had a maximum size of 120 nm with 4 spikes and the 667 nm in its LSPR. The GNS4 had a maximum size of

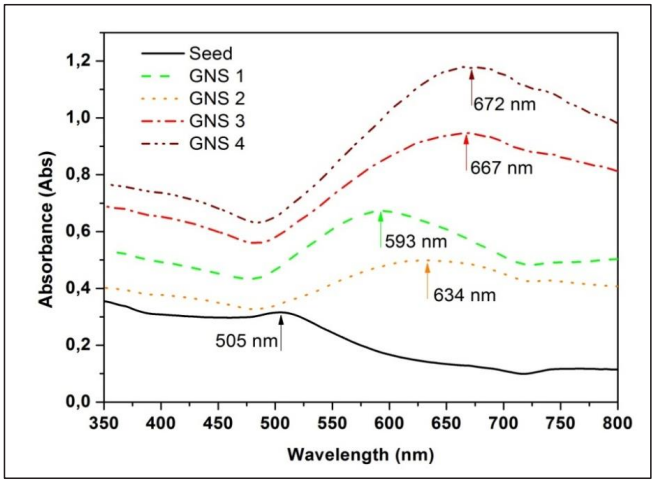

Fig. 5. Vis-NIR spectra of Au-seed and GNSs.

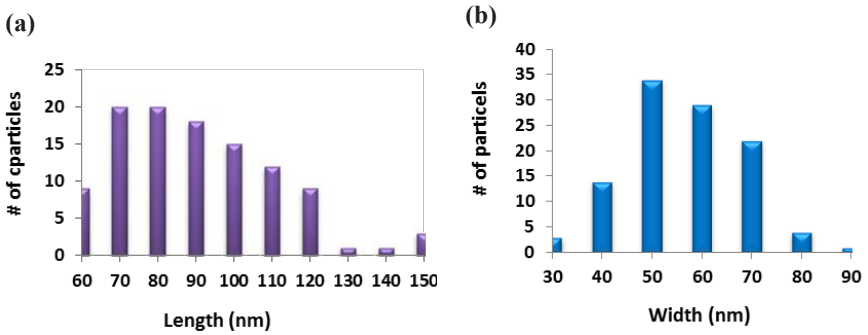

Fig. 6. Size distribution histograms of the (a) length of particles in GNS1, and (b) width of particles in GNS1.

140 nm with 5 branches and the 672 nm in its LSPR spectrum.

The size distribution histogram of the length and width of the particles in GNS1 has been shown in Fig. 6a and 6b, respectively. Both the length and width were measured at the outermost points of the stars. The mean value and standard deviation found for the length of the particles in GNS1 were 89.15 nm and 20.98 nm, respectively and mean value and STDEV of them were 55.73 nm and 11.88 nm, respectively. As it is seen in Fig. 7a, the mean value and standard deviation found for the length of GNS2 particles were 123 and 22 nm, respectively. The mean value and STDEV for the width of GNS2 were 87 nm and 19 nm as shown in Fig. 7b. In the same way, it is seen in Figs. 8a and 8b that the mean value and standard deviation found for the length of GNS3 are 126 and 23 nm, respectively and the mean value and STDEV for the width of them are 95 and 19 nm, respectively. The mean value and standard deviation found for the length of GNS4 particles in Fig. 9a were 148 and 10 nm, respectively. The mean value and STDEV for the width of GNS4 were 112 and 22 nm, respectively. Additionally, to comprehend the different optical responses from each GNS sample, it is necessary to investigate what the main differences are in terms of synthesis procedure and consequent structure in a more chronological procedure.

CONCLUSION

TEM images of synthesized gold nanostars showed a clear star-shape with at least 4 branches. The change of Au seed concentration in the growth solution influenced the size, spikes and the plasmonic peaks of GNSs. The lowest concentration of Au seed with volume percentage of 1.2% (GNS4) led to the largest particles with size of 140 nm. The defined shape and high yield for the sample

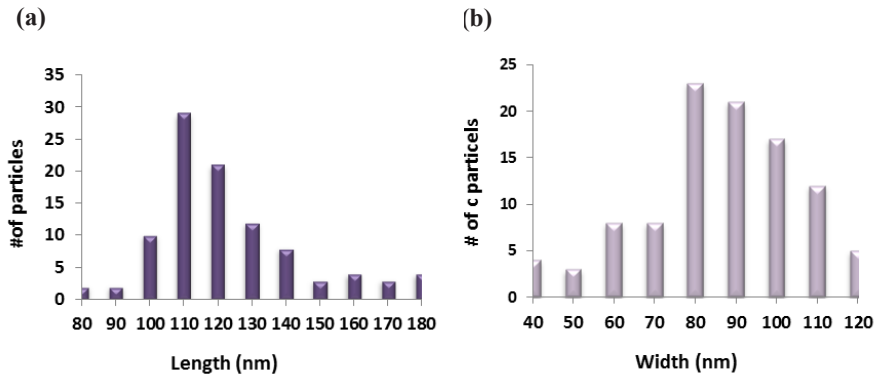

Fig. 7. Size distribution histograms of the (a) length of particles in GNS2, and (b) width of particles in GNS2.

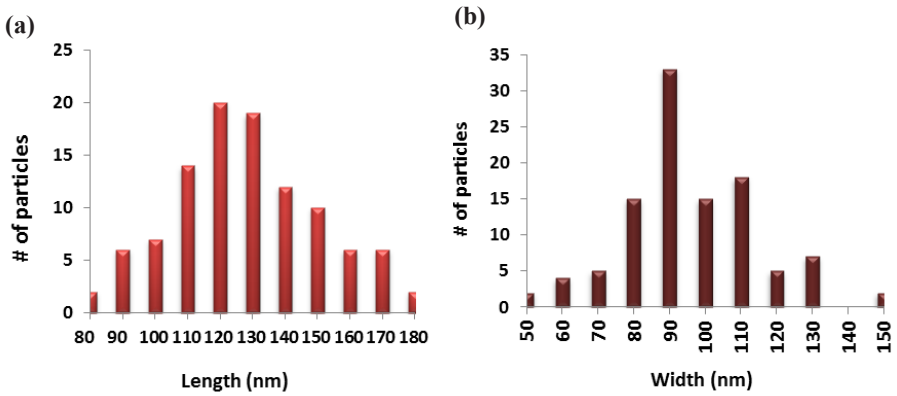

Fig. 8. Size distribution histograms of the (a) length of particles in GNS3, and (b) width of particles in GNS3.

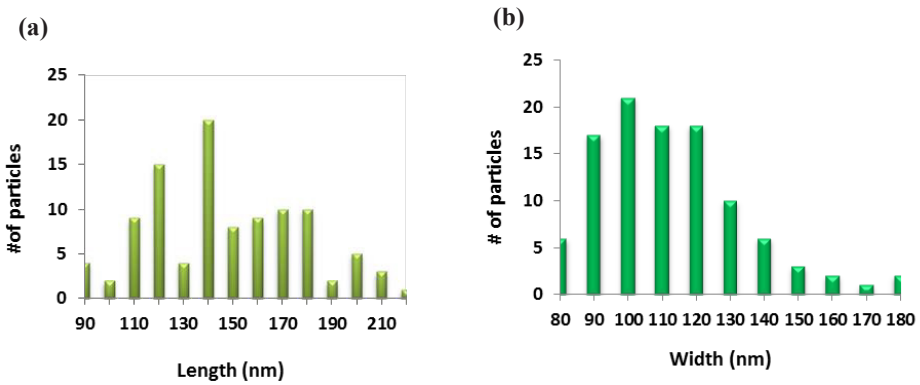

Fig. 9. Size distribution histograms of the (a) length of particles in GNS4, and (b) width of particles in GNS4.

with 1.9% Au seed (GNS3) can be attributed to the optimized condition of Ag combination with the seed in the growth solution. Ag in the presence of CTAB played a very important role in breaking the symmetry of seed particles by forming side branches initiating from AgBr molecules which surround the seed particle followed by formation of side branches which attach to AgBr. Moreover, the higher number of branches and the longer branch length were achieved for the GNS4 with the lowest amount of Au seed. Meanwhile, the wavelength of the samples' resonant plasmonic peaks of the absorption spectra red shifted with increasing the size and the number of side branches. The beneficial data was obtained using the seed mediated method and the synthesis of GNS was easily controllable and consistently reproducible.

CONFLICT OF INTEREST

The authors declare that there is no conflict of interests regarding the publication of this manuscript.

RFERENCES

1. Eustis S, El-Sayed MA. Why gold nanoparticles are more precious than pretty gold: Noble metal surface plasmon resonance and its enhancement of the radiative and nonradiative properties of nanocrystals of different shapes. Chem Soc Rev. 2006;35(3):209-217.
2. Choi HS, Ipe BI, Misra P, Lee JH, Bawendi MG, Frangioni JV. Tissue- and Organ-Selective Biodistribution of NIR Fluorescent Quantum Dots. Nano Lett. 2009;9(6):2354-2359.
3. Alvarez-Puebla R, Liz-Marzán LM, García de Abajo FJ. Light Concentration at the Nanometer Scale. The Journal of Physical Chemistry Letters. 2010;1(16):2428-2434.
4. Dam DHM, Culver KSB, Sisco PN, Odom TW. Research Spotlight: Shining light on nuclear-targeted therapy using gold nanostar constructs. Ther Deliv. 2012;3(11):1263-1267.
5. Webb JA, Bardhan R. Emerging advances in nanomedicine with engineered gold nanostructures. Nanoscale. 2014;6(5):2502.
6. Anker JN, Hall WP, Lyandres O, Shah NC, Zhao J, Van Duyne RP. Biosensing with plasmonic nanosensors. Nature Materials. 2008;7(6):442-453.
7. Butet J, Thyagarajan K, Martin OJF. Ultrasensitive Optical Shape Characterization of Gold Nanoantennas Using Second Harmonic Generation. Nano Lett. 2013;13(4):1787-1792.
8. Hrelescu C, Sau TK, Rogach AL, Jäckel F, Feldmann J. Single gold nanostars enhance Raman scattering. Appl Phys Lett. 2009;94(15):153113.
9. Yuan H, Khoury CG, Hwang H, Wilson CM, Grant GA, Vo-Dinh T. Gold nanostars: surfactant-free synthesis, 3D modelling, and two-photon photoluminescence imaging. Nanotechnology. 2012;23(7):075102.
10. Kang Z, Liu M, Li Z, Li S, Jia Z, Liu C, et al. Passively Q-switched erbium doped fiber laser using a gold nanostars based saturable absorber. Photonics Research. 2018;6(6):549.
11. Chung T, Lee S-Y, Song EY, Chun H, Lee B. Plasmonic Nanostructures for Nano-Scale Bio-Sensing. Sensors. 2011;11(11):10907-10929.
12. Wu Q, Sun Y, Ma P, Zhang D, Li S, Wang X, et al. Gold nanostar-enhanced surface plasmon resonance biosensor based on carboxyl-functionalized graphene oxide. Anal Chim Acta. 2016;913:137-144.
13. Pei Y, Wang Z, Zong S, Cui Y. Highly sensitive SERS-based immunoassay with simultaneous utilization of self-assembled substrates of gold nanostars and aggregates of gold nanostars. Journal of Materials Chemistry B. 2013;1(32):3992.
14. Li W, Chen X. Gold nanoparticles for photoacoustic imaging. Nanomedicine. 2015;10(2):299-320.
15. Barbosa S, Agrawal A, Rodríguez-Lorenzo L, Pastoriza-Santos I, Alvarez-Puebla RnA, Kornowski A, et al. Tuning Size and Sensing Properties in Colloidal Gold Nanostars. Langmuir. 2010;26(18):14943-14950.
16. Dreaden EC, Alkilany AM, Huang X, Murphy CJ, El-Sayed MA. The golden age: gold nanoparticles for biomedicine. Chem Soc Rev. 2012;41(7):2740-2779.
17. de Aberasturi DJ, Serrano-Montes AB, Liz-Marzán LM.

Modern Applications of Plasmonic Nanoparticles: From Energy to Health. Advanced Optical Materials. 2015;3(5):602-617.
18. Jana NR, Gearheart L, Murphy CJ. Seed-Mediated Growth Approach for Shape-Controlled Synthesis of Spheroidal and Rod-like Gold Nanoparticles Using a Surfactant Template. Adv Mater. 2001;13(18):1389-1393.
19. Jana NR, Gearheart L, Murphy CJ. Wet Chemical Synthesis of High Aspect Ratio Cylindrical Gold Nanorods. The Journal of Physical Chemistry B. 2001;105(19):4065-4067.
20. Nikoobakht B, El-Sayed MA. Preparation and Growth Mechanism of Gold Nanorods (NRs) Using Seed-Mediated Growth Method. Chem Mater. 2003;15(10):1957-1962.
21. New Frontiers of Nanoparticles and Nanocomposite Materials. Advanced Structured Materials: Springer Berlin Heidelberg; 2013.
22. Trigari S, Rindi A, Margheri G, Sottini S, Dellepiane G, Giorgetti E. Synthesis and modelling of gold nanostars with tunable morphology and extinction spectrum. J Mater Chem. 2011;21(18):6531.
23. Grzelczak M, Pérez-Juste J, Mulvaney P, Liz-Marzán LM. Shape control in gold nanoparticle synthesis. Chem Soc Rev. 2008;37(9):1783.
24. Senapati D, Singh AK, Khan SA, Senapati T, Ray PC. Probing real time gold nanostar formation process using two-photon scattering spectroscopy. Chem Phys Lett. 2011;504(1-3):46-51.